Overlapping resonances in the coherent control of radiationless transitions: Internal conversion in pyrazine

Cite as: J. Chem. Phys. **123**, 064313 (2005); https://doi.org/10.1063/1.2000260
Submitted: 06 April 2005 • Accepted: 23 June 2005 • Published Online: 17 August 2005

P. S. Christopher, Moshe Shapiro and Paul Brumer

Overlapping resonances in the coherent control of radiationless transitions: Internal conversion in pyrazine

P. S. Christopher
Chemical Physics Theory Group, Department of Chemistry, and Center for Quantum Information and Quantum Control, University of Toronto, Toronto, Ontario M5S 3H6, Canada

Moshe Shapiro
Department of Chemical Physics, The Weimann Institute of Science, Rehovot 76100, Israel and Department of Chemistry, University of British Columbia, Vancouver, British Columbia V6T 1Z1, Canada

Paul Brumer[a)]
Chemical Physics Theory Group, Department of Chemistry, and Center for Quantum Information and Quantum Control, University of Toronto, Toronto, Ontario M5S 3H6, Canada

(Received 6 April 2005; accepted 23 June 2005; published online 17 August 2005)

Coherent control of radiationless transitions is developed and applied to internal conversion. Conditions for active versus passive control are described and overlapping resonances are shown necessary for the phase control of radiationless transitions in molecular systems. Applications to pyrazine show the possibility of extensive control via optimized state preparation, as well as the significant role of overlapping resonances, even in the evolution of single vibrational states in S_2. © *2005 American Institute of Physics*. [DOI: 10.1063/1.2000260]

I. INTRODUCTION

Radiationless transitions[1,2] are ubiquitous processes that have been studied for over 70 years (see, e.g., Ref. 3 and references therein). They play a central role in energy and charge redistribution,[4] vision,[5] molecular electronics,[6] etc. Such processes result from the mixing of Born-Oppenheimer (BO) electronic surfaces via non-BO terms in the Hamiltonian. The resultant exact Hamiltonian eigenstates are therefore superpositions of states associated with each of the BO surfaces. Consequently, systems initiated on either BO surface undergo dynamics between the electronically coupled states.

Two conceptually similar types of radiationless transition processes are commonly distinguished: intersystem crossing and internal conversion (IC). They differ in the nature of the non-Born-Oppenheimer coupling; spin-orbit coupling is responsible for inducing intersystem crossing whereas nuclear-electronic coupling terms in the total Hamiltonian induce internal conversion. Frequently, radiationless transitions appear decaylike, proceeding irreversibly from one electronic surface to another, although oscillatory dynamics, manifest as beats, are also well known.

In this paper, we consider the coherent control[7,8] of radiationless transitions, i.e., the use of quantum interference, ostensibly induced by laser excitation, to manipulate the dynamics of such processes. Specifically, we show that by appropriately preparing a linear combination of zeroth-order states on one Born-Oppenheimer surface, quantum interference can be invoked to either maximize or minimize the population that undergoes a radiationless transition at a preset target time. Further, we show that successful phase control, i.e., control via variation of the phases of the initial superposition, requires the presence of overlapping resonances. This control methodology is then demonstrated on internal conversion in a relatively sophisticated model of pyrazine.[3,9,10] Note that pyrazine has long provided a model for studies of internal conversion.[3,11] As such, its dynamics and overlapping resonance structure are of particular, and possibly independent, interest.

Since it is not the central focus of this paper, the initial superposition state is assumed, in accord with the literature on shaped pulse,[12] to be preparable. For example, a desired state can be prepared via shaped laser pulsed excitation of the ground electronic state coupled with a wave-function diagnostic based upon time-resolved spontaneous emission.[13]

The approach that we advocate complements that of Sukharev and Seideman,[14] who have proposed suppression of radiationless transitions by exciting a superposition of bright states to prepare specific stationary eigenstates of the total Hamiltonian that are heavily localized on one electronic state.[15,16] The existence of such "extreme stationary states" allows for the suppression of radiationless transitions for extended time periods. This is a form of passive control, insofar as it relies entirely on the character and availability of these extreme eigenstates.

The work described below addresses the issue of control in the case where such states do not exist in the energy range of interest, or cannot be prepared radiatively due to the sparseness of the extreme states amongst a large state density.[17] In this case, as we show below, control over radiationless transitions is still possible. Further, this control relies heavily on the nature of overlapping resonances in the molecule. This perspective is a considerable extension of previous work[18] on overlapping resonances in the control of spon-

[a)]Electronic mail: pbrumer@tikva.chem.utoronto.ca

taneous emission, and we use it below to interpret the nature of the control achieved in time-dependent studies. In a subsequent paper[19] we adopt a frequency perspective, explicitly focus on the overlapping resonances contributions through a partitioning of Hilbert space, and apply the result to the control of intramolecular vibrational redistribution.

This paper is organized as follows. Section II A discusses the time-dependent approach to the coherent control of radiationless transitions and Sec. II B introduces the role of overlapping resonances. The method is then demonstrated in Sec. III for a four mode model of pyrazine (described in Sec. III A) where considerable control over internal conversion at fixed times is demonstrated. The aspects of resonances in pyrazine dynamics are described in Sec. III B and the control results are provided in Sec. IV. A summary in Sec. V concludes the paper and includes remarks on future proposed work on the nature of pyrazine models.

II. THEORY AND COMPUTATIONAL DETAILS

A. Time dependence

Consider a molecule with Hamiltonian given by

$$H = H_{\mathrm{ad}} + H_{12}, \tag{1}$$

where H is the total Hamiltonian, H_{ad} is the adiabatic Hamiltonian in which the coupling between electronic states is ignored, and H_{12} is the nonadiabatic coupling between electronic states. The eigenfunctions of the total Hamiltonian are denoted $|\gamma\rangle$, with

$$H_{\mathrm{tot}}|\gamma\rangle = E_\gamma|\gamma\rangle, \tag{2}$$

where the $|\gamma\rangle$ describe both electronic and nuclear motions. Below, we suppress all quantum indices pertaining to the rotational component of the dynamics, which is of little relevance to the radiationless processes of interest.

The dynamics of interest is that initiated in a vibrational state on one of the electronic surfaces, with probability flowing to the other electronic state. To this end we consider the eigenfunctions of H_{ad}, which are termed the "bare kets" and which are labeled with roman letters as $|i\rangle$, $|i'\rangle$, and $|j\rangle$. That is,

$$H_{\mathrm{ad}}|i\rangle = (E_i^{(e)} + E_i^{(v)})|i\rangle, \tag{3}$$

where $E_i^{(e)}$ is the electronic energy and $E_i^{(v)}$ is the vibrational energy associated with bare ket $|i\rangle$.

The dynamics is then initiated as a superposition of vibrational states on one electronic surface and the flow out of this electronic state is monitored. For notational simplicity we consider the case where the initial state is on an S_2 electronic state and the final state is on S_1, as in the case of pyrazine below; the discussion is, however, completely general.

The time-dependent probability $P_2(t)$ that the system is found in electronic state S_2 is given by

$$P_2(t) = \sum_{j\in S_2} |\langle j|\Psi(t)\rangle|^2, \tag{4}$$

where $|\Psi(t)\rangle$ is the state of the system at time t and the sum is over all bare kets that are in S_2. Consider then an initial state $|\Psi(0)\rangle$ that has been optically prepared on S_2 [i.e., $P_2(0)=1$] as

$$|\Psi(0)\rangle = \sum_{i\in S_2} c_i|i\rangle, \tag{5}$$

where c_i are the (complex) coefficients for the given initial state. Then, with the propagator $U(t)=e^{-iHt/\hbar}$, the state of the system at time t is

$$|\Psi(t)\rangle = U(t)|\Psi(0)\rangle = \sum_{i\in S_2} c_i U(t)|i\rangle, \tag{6}$$

and the quantity $P_2(t)$ is given by

$$P_2(t) = \sum_{j\in S_2} \left| \sum_{i\in S_2} c_i\langle j|U(t)|i\rangle \right|^2, \tag{7}$$

a form used later below.

Alternatively, using Eq. (6), expanding the square in Eq. (4), and collecting the coefficients c_i into a vector $\mathbf{c}$, we can rewrite Eq. (4) as

$$P_2(t) = \mathbf{c}^\dagger \mathbf{K} \mathbf{c}, \tag{8}$$

where the $\mathbf{K}$ matrix is given by

$$K_{i'i}(t) = \sum_{j\in S_2} \langle j|U(t)|i\rangle\langle j|U(t)|i'\rangle^*. \tag{9}$$

We consider coherently controlling $P_2(t)$ by preparing an initial vibrational superposition state on S_2 that either maximizes or minimizes $P_2(t)$ at some preselected target time T. [An analysis later below shows conditions under which this introduces quantum interference contributions to $P_2(t)$, hence displaying the essential feature of quantum control.[7]] Specifically, we seek the coefficients c_i that extremize $P_2(T)$ while preserving the norm of $\mathbf{c}$. To do so we introduce an undetermined multiplier, λ, and define

$$\xi(t,\mathbf{c}) = \mathbf{c}^\dagger \mathbf{K} \mathbf{c} - \lambda(\mathbf{c}^\dagger \mathbf{c} - 1). \tag{10}$$

The optimal set of initial coefficients (subject to the constraint on the norm) is then found for stationary $\xi(t,\mathbf{c})$, i.e., when

$$\begin{aligned} \frac{\partial \xi(t,\mathbf{c})}{\partial\, \mathrm{Re}[c_i]} &= 0, \\ \frac{\partial \xi(t,\mathbf{c})}{\partial\, \mathrm{Im}[c_i]} &= 0, \end{aligned} \tag{11}$$

for λ, the real ($\mathrm{Re}[c_i]$), and imaginary ($\mathrm{Im}[c_i]$) parts of c_i for all i. Equation (11) is equivalent to the eigenvalue problem

$$\mathbf{K}(t)\mathbf{c} = \lambda \mathbf{c}. \tag{12}$$

Hence, the optimum initial coefficients for time T are determined by diagonalizing $\mathbf{K}(T)$.

To understand the nature of the dynamics we expand Eq. (8) and collect appropriate terms to rewrite P_2 as

$$P_2(t) = \sum_i |c_i|^2 g_i(t) + \sum_{i\neq i'} c_{i'}^* c_i f_{ii'}(t), \tag{13}$$

with

$$g_i(t) = \sum_{j\in S_2} |\langle j|U(t)|i\rangle|^2,$$
$$f_{ii'}(t) = \sum_{j\in S_2} \langle j|U(t)|i\rangle\langle j|U(t)|i'\rangle^*. \tag{14}$$

Equations (13) and (14) admit simple interpretations: g_i describes the P_2 dynamics of a system that is initially prepared as the bare ket $|i\rangle$, whereas $f_{ii'}$ provides the effect of interferences between the bare kets comprising the initial superposition state $|\Psi(0)\rangle$. This structure is typical of coherent control, i.e., direct contributions from independent pathways, plus interference terms between them. Hence, comparatively large values of $f_{ii'}(T)$ indicate that interference is playing a significant role in the pyrazine dynamics at the target time, and that *phase control*, i.e., the ability to control $P_2(t)$ via the *phases* of the coefficients c_i, is possible. By contrast, if the g_i terms dominate then active control over the P_2 dynamics is not possible for the energy regime spanned by $|\Psi(0)\rangle$. In this case only "passive" control is possible, where one weights, in $|\Psi(0)\rangle$, the specific $|i\rangle$ whose decay is slowest (for suppression of P_2 decay) or fastest (for enhancement of P_2 decay).

Additional insight into $P_2(t)$ utilized below is gained from the perspective of the exact eigenstates $|\gamma\rangle$. Specifically, by substituting Eq. (6) into Eq. (4) and using $\Sigma_\gamma|\gamma\rangle\langle\gamma|=1$ in conjunction with the definition of the propagator, $U(t)=\Sigma_\gamma|\gamma\rangle\exp(-iE_\gamma t/\hbar)\langle\gamma|$, we get

$$P_2(t) = \sum_{j\in S_2}\left|\sum_{i\gamma} c_i\langle j|\gamma\rangle\langle\gamma|i\rangle e^{-(iE_\gamma t/\hbar)}\right|^2$$
$$= \sum_{j\in S_2}\sum_{i\gamma i'\gamma'} c_i c_{i'}^*\langle j|\gamma\rangle\langle\gamma|i\rangle\langle i'|\gamma'\rangle\langle\gamma'|j\rangle e^{-[i(E_\gamma - E_{\gamma'})t]/\hbar}. \tag{15}$$

Further, we note that the infinite time average $\bar{h}$,

$$\bar{h} = \lim_{T\to\infty}\frac{1}{T}\int_0^T h(t)dt, \tag{16}$$

of various quantities $h(t)$ proves be of use below. For example, using Eq. (15), $\bar{P}_2$ is given by

$$\bar{P}_2 = \sum_{j\in S_2}\sum_{i\gamma i'} c_i c_{i'}^*|\langle j|\gamma\rangle|^2\langle i'|\gamma\rangle\langle\gamma|i\rangle, \tag{17}$$

since only $\gamma=\gamma'$ terms contribute. Note, as in all infinite time averages, given knowledge of the kets $|\gamma\rangle$, the evaluation of $\bar{P}_2$ requires no time integration.

Finally, we note an alternative probability,

$$P_2'(t) = \sum_{j\in A}\left|\sum_{i\in A} c_i\langle j|U(t)|i\rangle\right|^2, \tag{18}$$

where A is a subset of S_2. Here $P_2'(t)$ gives the probability of remaining in the initial subspace A of S_2. The most elementary of these cases:

$$P_2''(t) = |\langle i|U(t)|i\rangle|^2, \tag{19}$$

which provides the probability of staying within just a single created bare ket $|i\rangle$, is also of interest below.

B. Resonances

Examining the character of the resonances associated with the control of internal conversion will provide useful insights into the nature of control. Note that in simple model IC cases a single bare ket is excited and other S_2 states are regarded as irrelevant, so that Eq. (13) takes the form

$$P_2(t) = \left|\sum_\gamma |\langle i|\gamma\rangle|^2 e^{-iE_\gamma t/\hbar}\right|^2. \tag{20}$$

If the coefficients $|\langle i|\gamma\rangle|^2$ are distributed as a Lorentzian in E_γ, and the level spacing is tiny, the decay of $P_2(t)$ is exponential. More complex, however, and more relevant to the discussion below, is the case where there are several neighboring resonances that are wider than the adjacent level spacing, so that the resonances overlap. That is, two or more bare kets have nonzero overlap matrix elements with the same $|\gamma\rangle$. The resulting resonances (see, e.g., Fig. 6.13 in Ref. 7) interfere with one another and display a variety of shapes, including the appearance of "dark" regions where absorption is zero.[20]

Consider then Eq. (14). The interference term $f_{ii'}(t)$ depends upon

$$\langle j|U(t)|i\rangle\langle j|U(t)|i'\rangle^* = \sum_{\gamma,\gamma'}\langle j|\gamma\rangle\langle\gamma|i\rangle\langle i'|\gamma'\rangle \times\langle\gamma'|j\rangle e^{-i(E_\gamma - E_{\gamma'})/\hbar}. \tag{21}$$

Therefore nonzero $f_{ii'}(t)$, and hence the ability to control the system via the phases of the c_i, requires that at least two bare kets have nonzero overlap with at least one common exact eigenstate, i.e., that there are overlapping resonances. Note, however, that the overlap need not occur between the bare kets comprising the original superposition state [Eq. (5)].

The specific case where there are only two relevant bare kets $|1\rangle$ and $|2\rangle$ in both the initial superposition and in the final target space, i.e., an example of the $P_2'(t)$ case above, yields an interesting corollary result. Specifically, in this case all of the bare states considered (in either the initial superposition or in the final target space A) are either $|1\rangle$ or $|2\rangle$. Hence, via Eq. (21), successful phase control requires that the bare kets in the initial superposition are a pair of overlapping resonances.

Overlapping resonances contribute as well to the "direct" g_i contribution in Eq. (14) since they affect the nature of the decay from individual $|i\rangle$. Specifically, they distort the line shape, and hence the corresponding time dependence, away from the simple behavior expected from a Lorentzian line. Hence, a quantitative measure of the contribution of the overlapping resonances to $P_2(t)$ is difficult to construct. However, to qualitatively assess the overall role of the overlapping resonances in the $P_2(t)$ dynamics we consider the following diagnostic:

$$W(t) = \sum_{j\in S_2}|c_j\langle j|U(t)|j\rangle|^2. \tag{22}$$

In the limiting case of no overlapping resonances, via Eq. (7), $P_2(t)=W(t)$. Hence, here we adopt $W(t)$ as a measure of the nonoverlapping resonance contribution to $P_2(t)$, and $P_2^{\text{or}}(t)=[P_2(t)-W(t)]$ as a measure of the overlapping reso-

nance contribution. Neither are exact representations of the role of the resonances insofar as the existence of overlapping resonances also affects the time dependence of the diagonal terms $\langle j|U(t)|j\rangle$.

III. CONTROL OF INTERNAL CONVERSION IN PYRAZINE

A. Pyrazine molecule

The dynamics of pyrazine is treated using a model due to Borrelli and Peluso[10,21] that was inspired by Woywod *et al.*[9] Here, the $|i\rangle$ are products of an electronic component, either of the S_1, or S_2 electronic state, and a vibrational part, which is itself a product of harmonic-oscillator (HO) eigenfunctions; one HO eigenfunction for each of the 24 normal modes of the molecule. Although all 24 modes are included in the calculation, nonzero quantum numbers are allowed in only four of these modes. Specifically, excitations of the 1, 6*a*, 8*a*, and 10*a* modes of up to 10, 9, 8, and 9 quanta, respectively, are included (i.e., we include every HO products that has mode 1 with a quantum number not exceeding 10, and mode 6*a* with a quantum number not exceeding 9, etc.). The S_1 to S_2 coupling is given by the simple linear term:

$$H_{12} = \beta Q_{10a}, \tag{23}$$

where Q_{10a} is the 10*a* normal coordinate and

$$\beta = 1.3\left(\frac{\text{eV}}{\text{Å(amu)}^{1/2}}\right), \tag{24}$$

obtained via a qualitative fit to experimental data. The difference in electronic energy is taken as

$$|E_{S_1}^{(e)} - E_{S_2}^{(e)}| = 0.956 \text{ eV}. \tag{25}$$

Given the basis, the eigenvectors of the total Hamiltonian were determined via standard linear algebra techniques. A total of 9900 bare kets on each of the S_2 and S_1, surfaces were utilized, constructed as described above. States on S_1 are consecutively labeled as $|1\rangle$ to $|9900\rangle$ and those on S_2 are labeled $|9901\rangle$ to $|19\,800\rangle$.

Throughout this study we are cognizant of the fact that the density of states of both S_2 and S_1 are far lower in the four-mode pyrazine model than they would be in the full 24-mode molecule. This difference is particularly acute for the S_1 surface which lies lower in energy than S_2. As a consequence, the initially created S_2 superposition decays into an unrealistically low S_1 density of states. Whether this affects the dynamics or not depends upon whether the correct dynamics is "tierlike"[22] in which case it would suffice, over some time scale, to include only the states included here, i.e., those directly coupled to the S_2 states. Evaluation of the importance of this density of states issue to both the $P_2(t)$ dynamics and to the existence of "extreme" states $|\gamma\rangle$ that are heavily weighted (or lightly weighted)[14] on S_2 is under study.[23] For the current paper we note, however, that our model contains four modes, larger than other eigenstate studies of pyrazine dynamics in the literature.

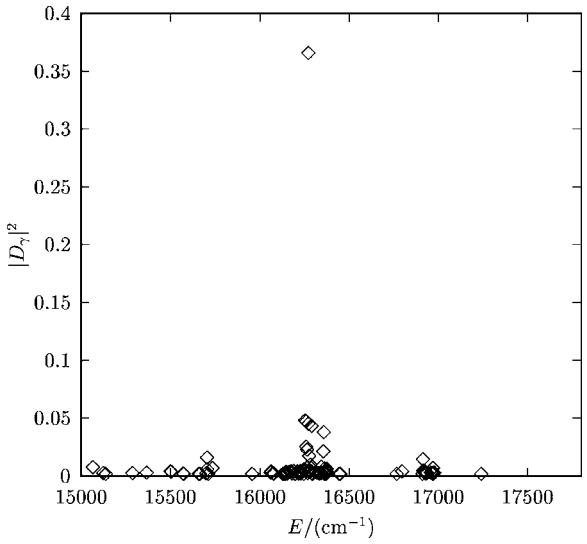

FIG. 1. Narrow resonance shape—ket $|11\,432\rangle$.

B. Resonances in pyrazine

The static computations of the bare kets $|i\rangle$ and the exact eigenstates $|\gamma\rangle$ yield direct information on the nature of the resonances in this model of pyrazine. If we expand a bare ket, $|i\rangle$, in the exact eigenstates, $|\gamma\rangle$:

$$|i\rangle = \sum_\gamma D_\gamma |\gamma\rangle, \tag{26}$$

then the line shape $|D_\gamma|^2 = |\langle\gamma|i\rangle|^2$ versus energy provides a picture of the resonance.

Figures 1 and 2 show two typical example of the resonance shapes observed in these calculations, here for states $|11\,432\rangle$ and $|10\,088\rangle$. The former appears sharp and single peaked, being spread out over a few hundred wave numbers. By contrast, the latter shows at least two peaks regions and is broadly distributed over several thousand wave numbers. The latter are clearly distorted from a simple line shape,

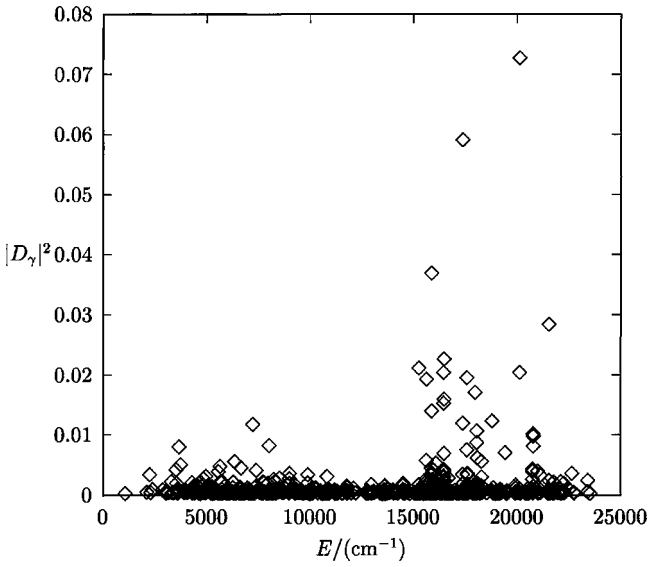

FIG. 2. Wide resonance shape—ket $|10\,088\rangle$.

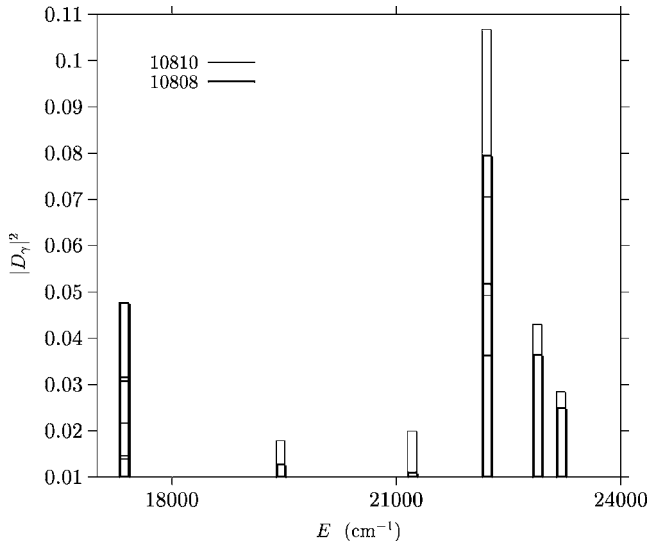

FIG. 3. Overlap of states $|10\,808\rangle$ and $|10\,810\rangle$. Shown are the maximum $|D_\gamma|^2$ contributions, as histogram heights, for the two indicated kets. The histogram boxes with several horizontal lines indicated more than one exact eigenstate contributing in that energy region.

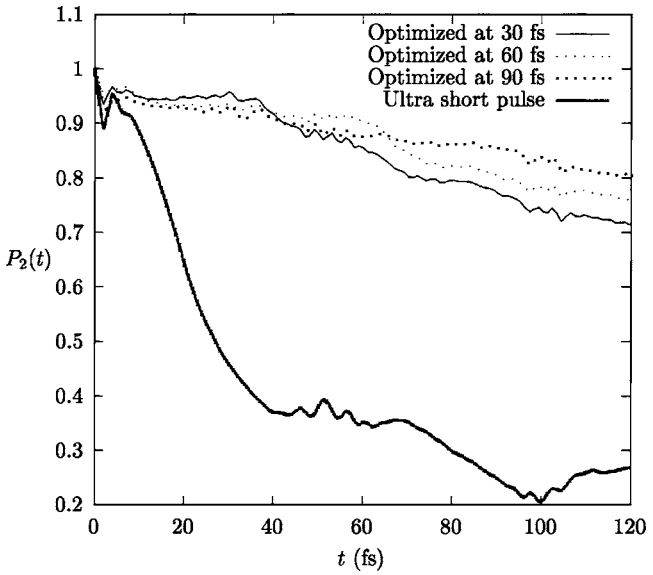

FIG. 4. $P_2(t)$ for a state prepared with an ultrashort pulse and for three optimized states.

reflective of overlapping resonances. As we will see below, $|11\,432\rangle$ is also affected by the presence of other bare kets.

Note, significantly, that there are many "gaps" in each of these line shapes, i.e., exact eigenstates whose $|D_\gamma|^2$ is negligible, distributed amongst those with nonzero values. This gap structure is significant with respect to the issue of overlapping resonances, which requires that specific $|\gamma\rangle$ have nonzero overlap matrix elements with more than one $|i\rangle$. That is, the "picket-fence-like" structure of the line shapes that we observe makes the overlap weaker than would be the case if the line shapes were fully filled.

An examination of the nature of these "missing" eigenstates showed no specific trends responsible for the low $|D_\gamma|^2$. In particular, there were no obvious symmetry reasons for these small projections. Further studies will be necessary to examine whether increasing the number of modes in the model will fill in these gaps.[23] Overlaps of lines typical of those observed are shown in Fig. 3, which is discussed in further detail below.

Also observed in this model of pyrazine are the bare kets that almost entirely comprise a single exact Hamiltonian eigenstate, i.e., eigenstates that are comprised of over 90% of one bare ket. The dynamics of these extreme states has been emphasized by Sukharev and Seideman.[16]

IV. RESULTS

A. Controlled $P_2(t)$

The typical computed $P_2(t)$ curves displayed behavior qualitatively described by two regions: region I where the $P_2(t)$ decays essentially monotonically, followed by region II where $P_2(t)$ tends to oscillate around $\bar{P}_2$. The time scale for passing from region I to region II depends on the initial state. A specific $P_2(t)$ decay obtained upon delta pulse laser excitation of a superposition of vibrational states of S_2 from S_0 is shown as a solid line in Fig. 4. Here the pulse created a superposition primary composed of the 50 bare kets with the largest Franck-Condon factors that connect S_0 with S_2. The resultant initial wave packet is centered at $\approx$9500 cm^{-1} with a width of 990 cm^{-1}. (Throughout this paper, the zero in energy is the ground vibrational state of the S_1 surface which is 4.95 eV above the ground vibrational state of the S_0 surface.) The decay is rapid, on the time scale of 20–40 fs, consistent with experimental results.[24]

Figure 4 also shows the $P_2(t)$ resulting from the maximization of $P_2(T)$ decay for three cases, obtained in accord with the procedure outlined in Sec. V. These results use the same 50 bare kets that comprise the above short pulse initial state, and differ only by the times at which they were maximized: $T=30$, 60, or 90 fs, respectively. An examination of the composition of these three states shows the origin of their similarity: approximately 80% of the amplitude of each initial state lies in only one bare ket—that bare ket with the largest $\bar{P}_2$. As a secondary effect, amplitude is distributed amongst the remaining forty-nine states, in order to maximize $P_2(T)$. Hence, the maximization of $P_2(T)$ here emerges primarily from a single g_i contribution of Eq. (14), but using states conceptually similar to, but quantitatively different than those observed by Sukharev and Seideman[14] insofar as they are shorter lived. Little, if any, active interference-based coherent control participates in these optimizations. Similar observations were made for the case of $P_2(T)$ minimizations.

To demonstrate active control in this model of pyrazine therefore requires that we focus on those bare kets that have a fairly large $f_{ii'}(t)$ value at the target time of interest. Actually selecting the bare kets with this property is a nontrivial task, because computing $f_{ii'}(t)$ as a function of time for the 9900 bare kets on S_2 is computationally prohibitive. To resolve this issue we computed the infinite time average $\bar{f}_{ii'}$ for sets of states and selected a family of bare kets based on the magnitudes of this quantity. Numerous published shaped-pulse studies make clear that such a superposition can be created experimentally via proper pulse shaping.

Consider first a case where the initial superposition is

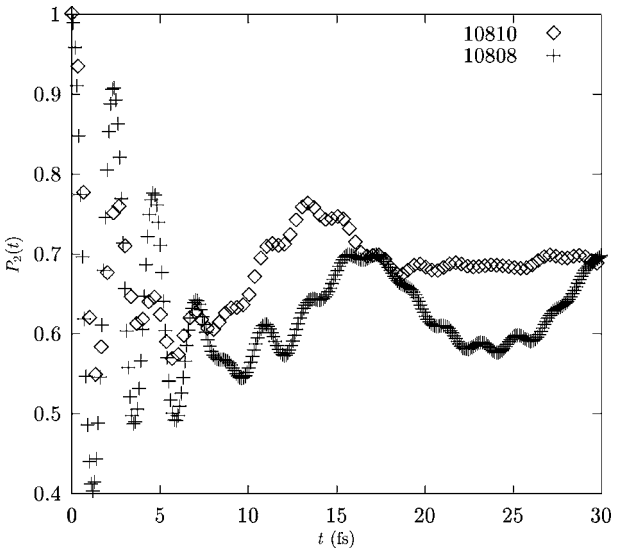

FIG. 5. Individual time evolution of P_2 for each of the levels $|10\,810\rangle$ and $|10\,808\rangle$.

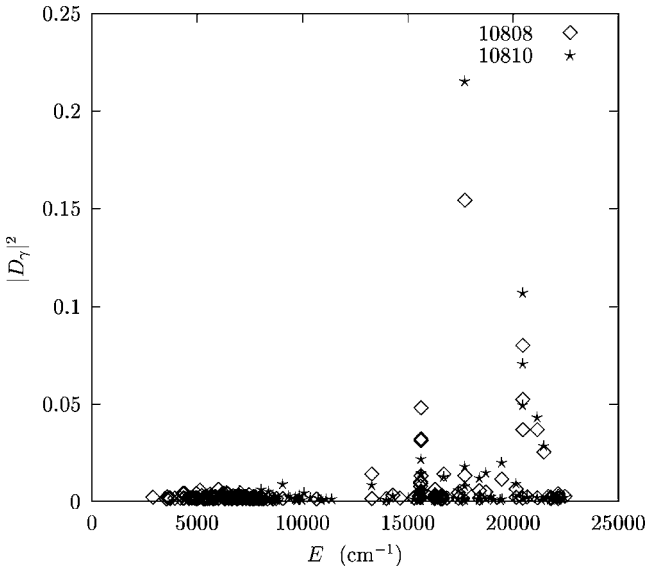

FIG. 7. Resonance shape of $|10\,808\rangle$ and $|10\,810\rangle$.

comprised only two bare kets, $|i\rangle=|10\,810\rangle$ and $|i'\rangle=|10\,808\rangle$. The time evolution of each of these kets, regarded independently, is shown in Fig. 5. Note that neither of these states display a simple falloff of $P_2(t)$, but rather show population that oscillates in and out of S_2, leading to a long-time value of $P_2\approx 0.68$. This type of quasiperiodic dynamics was typical of most of the states studied, and is possibly due to the low density of states on the S_1 surface.

As a control example consider optimizing $P_2(t)$ using an initial superposition of two states $|10\,808\rangle$ and $|10\,810\rangle$ at $T=20$ fs. The results are shown in Fig. 6. Here the difference between the maximal and minimal $P_2(t)$ at this target time is seen to be significant, but not substantial. That is, the maximum $P_2(T)$ is 0.75 whereas the minimum is 0.52. Such control arises from the participation of overlapping resonances in the S_2 manifold, with the individual bare states shown in Fig. 7. The primary contributions to the overlap of these two states is shown in Fig. 3, where the height of the histogram indicates the contribution of each of the bare kets to the exact state at the indicated energy E_γ.

A considerably different degree of control obtains from optimizing the probability, $P_2'(t)$, of remaining within the two states $|10\,808\rangle$ and $|10\,810\rangle$, which we here use to define the subspace A. The results of optimization at either $T=15$ and 20 fs are visually indistinguishable and are shown in Fig. 8. These results should be compared to the uncontrolled probability of each of the two states $|10\,808\rangle$ and $|10\,810\rangle$ remaining solely within this manifold, as shown in Fig. 9. Two things are evident. First, the individual $P_2'(t)$ curves lie far lower than those in Fig. 6, indicating the participation of many more bare kets in the dynamics of $P_2(t)$ than merely the two bare kets that form this original superposition. Second, with these few states, the extent of control depends heavily on the target time T: control at $T=15$ fs is clearly far

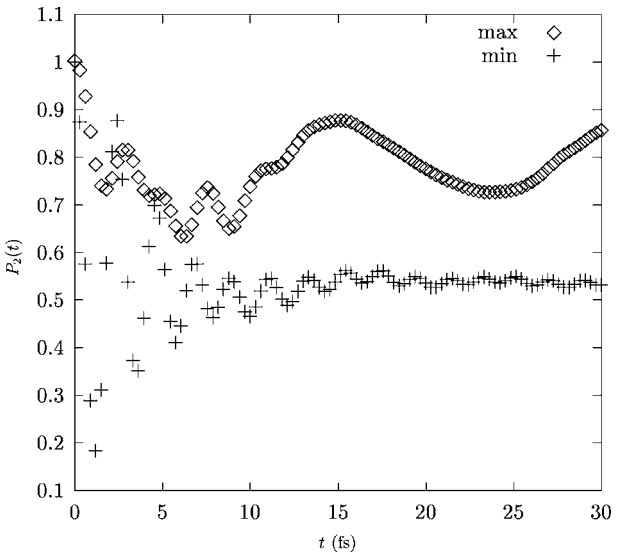

FIG. 6. Superposition of $|10\,808\rangle$ and $|10\,810\rangle$: P_2 optimized at $T=20$ fs.

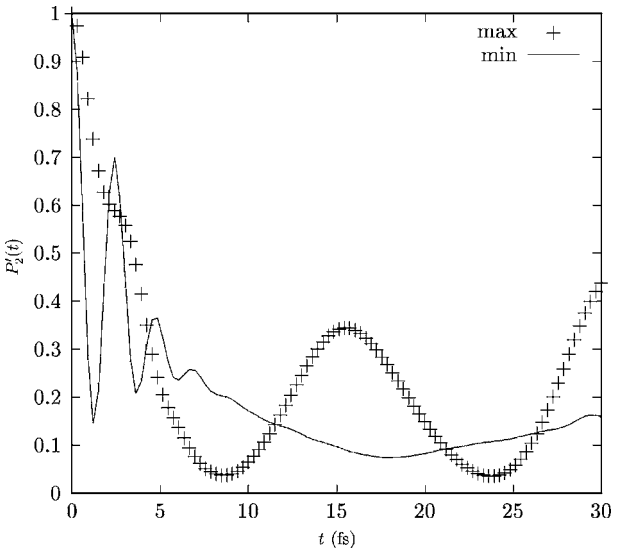

FIG. 8. Optimized P_2' curves for $|10\,808\rangle$ and $|10\,810\rangle$. Optimization time $T=15$ or 20 fs.

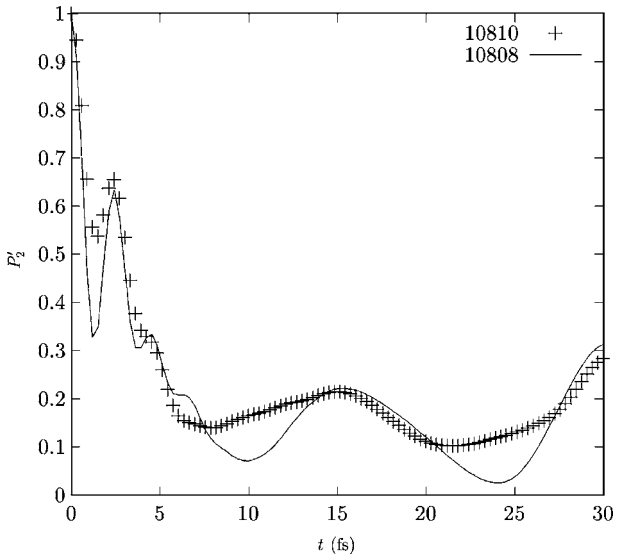

FIG. 9. Individual P_2' curves for $|10\,808\rangle$ and $|10\,810\rangle$.

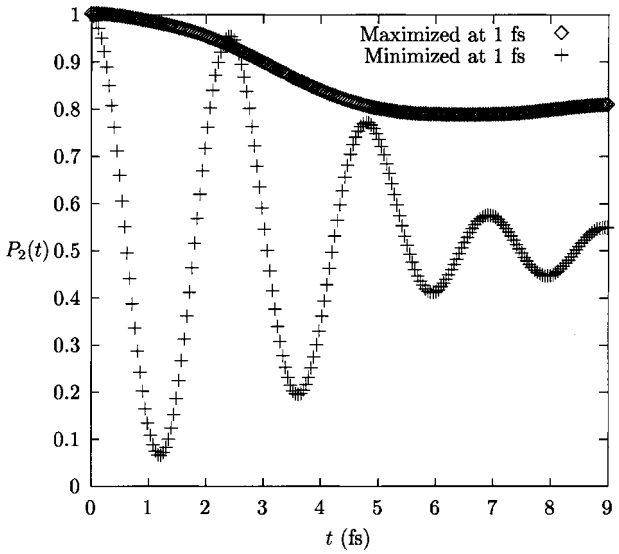

FIG. 11. Same as Fig. 10 except that optimizations were performed at 1 fs.

better than that at $T=20$ fs, a manifestation of the time-dependent component of the interference contribution to $f_{ii'}$.

$P_2(t)$ control results are significantly better when a much larger set of initial states forms the superposition state. Two such results, using 100 states centered $\approx 18\,000$ cm^{-1} with a width of ≈ 2000 cm^{-1}, are shown in Figs. 10 and 11. Optimizations at both $T=10$ fs and $T=1$ fs are shown. There is appreciable control in both cases, i.e., there is now a considerable difference between the population of the maximized and minimized curves. This is particularly true for the 1-fs case, where $P_2(t)$ varies over the range of 90%. Note also that the maximized $P_2(t)$ persists at high values well beyond 1 fs. Similarly, control in the 10-fs case is large, ranging from $P_2(T=10)$ of 0.9 to 0.54.

These optimization results are typical of those obtainable within this model of pyrazine, and are suggestive of the feasibility of coherent control in the real pyrazine system.

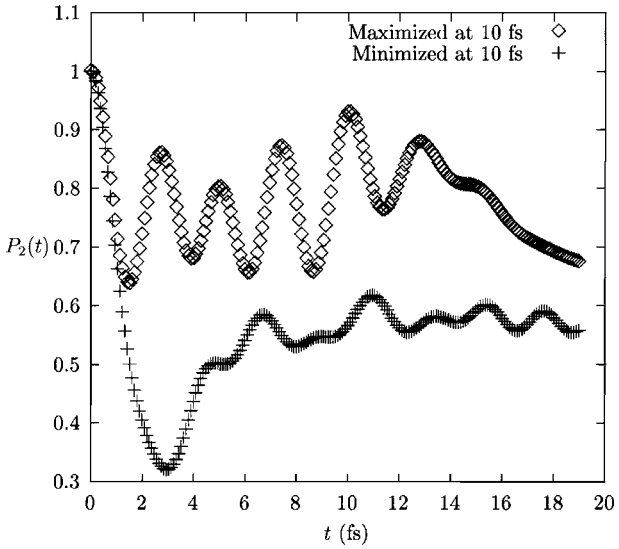

FIG. 10. Maximized and minimized populations at 10 fs for a family of bare kets that have relatively large $\bar{f}_{ii'}$.

B. Overlapping resonances contribution: $W(t)$

Equation (22) provided a qualitative measure of the extent to which overlapping resonances contribute to the optimization. Table I shows the values of $W(T)$ and $P_2^{\mathrm{or}}(T) = [P_2(T) - W(T)]$ for several of the $P_2(T)$ optimizations discussed above. Results for $P_2'(T)$ optimizations are not considered because they add little to these results.

TABLE I. Comparison of overlapping and nonoverlapping resonance contribution to control for various control cases. (A) Maximization of $|10\,810\rangle$ and $|10\,808\rangle$. (B) Minimization of $|10\,810\rangle$ and $|10\,808\rangle$. (C) Maximization of the collection of states of Figs. 10 and 11. (D) Minimization of the collection of states of Figs. 10 and 11. (E) Maximization of a poorly interfering collection of states, primarily $|11\,432\rangle$.

(A)	T	P_2	W	P_2^{or}
	1.0	0.845	0.478	0.366
	10.0	0.740	0.087	0.652
	30.0	0.865	0.038	0.826
(B)	T	P_2	W	P_2
	1.0	0.216	0.417	−0.201
	10.0	0.461	0.0571	0.403
	30.0	0.519	0.038	0.481
(C)	T	P_2	W	P_2^{or}
	10.0	0.927	0.078	0.849
	20.0	0.928	0.134	0.793
	70.0	0.867	0.034	0.832
	100.0	0.935	0.171	0.765
(D)	T	P_2	W	P_2^{or}
	10.0	0.360	0.161	0.199
	20.0	0.387	0.038	0.349
	70.0	0.236	0.030	0.206
	100.0	0.224	0.020	0.204
(E)	T	P_2	W	P_2^{or}
	1.0	0.929	0.925	0.004
	20.0	0.920	0.495	0.424
	60.0	0.863	0.597	0.265
	100.0	0.787	0.192	0.594

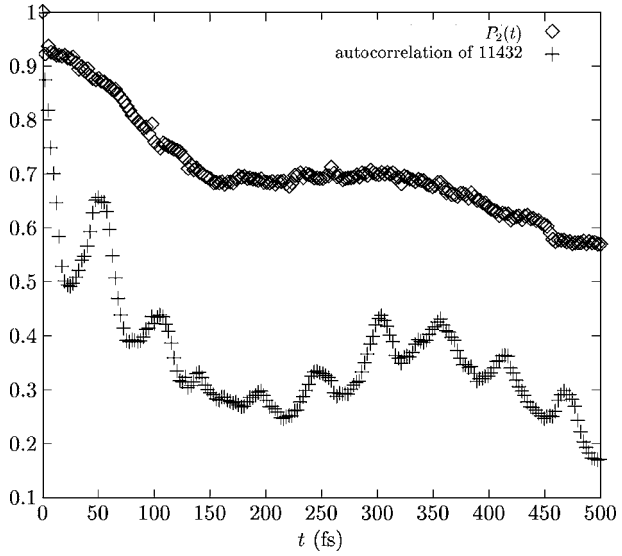

FIG. 12. $P_2(t)$ and $P_2''(t)$ for the initial state $|11\,432\rangle$.

The table clearly shows that, at all indicated (long) target times, the overlapping resonances contribution is the overwhelming contribution to $P_2(T)$ for optimizations starting with a two ket superposition. However, an examination of the details finds it difficult to correlate the degree of control with the size of the $P_2^{\mathrm{or}}(T)$ contribution. The origin of this problem becomes clear when examining the behavior of those single states that sometimes emerge as the dominant contribution to a superposition when optimizing $P_2(T)$. An example is shown in Fig. 12. Here the upper curve shows $P_2(t)$ for $\Psi(0)=|11\,432\rangle$, a state whose resonance structure is shown in Fig. 1. Upon optimization of $P_2(t)$ in the energy region of this state, for optimization times up to $T=100$ fs, $|11\,432\rangle$ is found to dominate the optimized superposition and $P_2(t)$ is found to decay rather slowly, looking very much like the upper curve in Fig. 12. However, despite the fact that only a single state dominates the superposition, P_2^{or} is found to be large for this optimization being ≈ 0.2–0.65. The latter suggests that, despite the narrowness of the $|11\,432\rangle$ line shape [see Fig. 1], there are significant overlapping resonances contributions to the $P_2(t)$ dynamics of this single ket. This proposal is confirmed by the lower curve in Fig. 12 which shows $P_2''(t)$ for the state $|11\,432\rangle$. This quantity, the autocorrelation function of the state $|11\,432\rangle$, falls off far more rapidly than does $P_2(t)$. A comparison of Eqs. (4) and (19) with $|\Psi(0)\rangle=|i\rangle=|11\,432\rangle$ shows that the difference between $P_2(t)$ and $P_2''(t)$ lies in the contribution of states other than $|11\,432\rangle$ to the sum over final S_2 states. The fact that $P_2''(t)$ lies lower than $P_2(t)$ in Fig. 12 is then due to the fact that the initial state $|11\,432\rangle$ overlaps the $|\gamma\rangle$ states that in turn overlap other bare kets $|j\rangle$, i.e., that other resonances overlap $|11\,432\rangle$. It therefore appears that overlapping resonances play a role even in the decay of a single state, making it difficult to extract a quantitative relationship between the extent of control in a prepared superposition and the contribution from overlapping resonances.

V. SUMMARY

Control of radiationless transitions in general has been discussed in detail in this paper, and a methodology described to optimize radiationless processes at fixed times. In addition, the direct connection between the existence of overlapping resonances and the possibility of phase control via the coefficients of a prepared superposition on a Born-Oppenheimer electronic surface has been established.

The paper has also presented specific applications to internal conversion in pyrazine. A four-mode model of pyrazine has been used, and high quality control has been demonstrated. We plan additional studies to try and significantly increase the density of states in both the S_2 and S_1 manifolds while still retaining an energy eigenvalue perspective. Of particular interest in control studies using these higher dimensional systems will be the question of whether recurrences in $P_2(t)$ are seen as readily with the higher dimensionality system, and whether extreme states, such as those emphasized by Sukharev and Seideman, continue to play a significant role as the state density increases. Studies of this kind are currently ongoing.[23]

ACKNOWLEDGMENTS

One of the authors (P.S.C.) gratefully acknowledges R. Borrelli and A. Peluso for various input data as well as for wise advice on the pyrazine model during the course of this work. This work was supported by grants from the Natural Sciences and Engineering Research Council Canada and Photonics Research Ontario.

[1] E. S. Medvedec and V. I. Osherov, *Radiationless Transitions in Polyatomic Molecules* (Springer, Berlin, 1995).
[2] K. F. Freed, Top. Appl. Phys. **15**, 23 (1976).
[3] J. Kommandeur, W. A. Majewski, W. L. Meerts, and D. W. Pratt, Annu. Rev. Phys. Chem. **38**, 433 (1987).
[4] J. Hichl and V. Bonacic-Koutecky, *Electronic Aspects of Organic Photochemistry* (Wiley, New York, 1990).
[5] R. W. Schoenlein, L. A. Peteanu, R. A. Mathies, and C. V. Chank, Science **254**, 412 (1991).
[6] J. Jortner and M. A. Ratner, *Molecular Electronics* (Blackwell Science, Oxford, 1997).
[7] M. Shapiro and P. Brumer, *Principles of the Quantum Control of Molecular Processes* (Wiley, New York, 2003).
[8] S. A. Rice and M. Zhao, *Optical Control of Molecular Dynamics* (Wiley, New York, 2000).
[9] C. Woywod, W. Domcke, A. L. Sobolewski, and H. J. Werner, J. Chem. Phys. **100**, 1400 (1994).
[10] R. Borrelli and A. Peluso, J. Chem. Phys. **119**, 8437 (2003).
[11] See, e.g., B. J. Van der Meer, H. T. Jonkman, G. M. ter Horst, and J. Kammandeur, J. Chem. Phys. **76**, 2099 (1982); A. Lorincz, D. D. Smith, F. Novak, R. Kosloff, D. J. Tannor, and S. A. Rice, *ibid.* **82**, 1067 (1985); F. Novak, R. Kosloff, D. J. Tannor, A. Lorincz, D. D. Smith, and S. A. Rice, *ibid.* **82**, 1073 (1985); M. Thoss, W. H. Miller, and G. Stock, *ibid.* **112**, 10282 (2005), and references therein.
[12] See, e.g., T. Brixner and G. Gerber, ChemPhysChem **4**, 418 (2003).
[13] M. Shapiro, J. Chem. Phys. **103**, 1748 (1995); Chem. Phys. **207**, 317 (1996).
[14] M. Sukharev and T. Seideman, Phys. Rev. Lett. **93**, 093004 (2004).
[15] M. Shapiro and M. S. Child, J. Chem. Phys. **76**, 6176 (1982).
[16] G. Hose and H. S. Taylor, Chem. Phys. **84**, 375 (1984).
[17] Such extreme states, known from studies of intramolecular vibrational redistribution, are expected to become an increasingly smaller fraction of the total density of states in the semiclassical limit.

[18] E. Frishman and M. Shapiro, Phys. Rev. Lett. **87**, 253001 (2001).
[19] D. Gerbasi, P. Christopher, A. Sanz, M. Shapiro, and P. Brumer (unpublished).
[20] M. Shapiro, J. Chem. Phys. **56**, 2582 (1972).
[21] The Franck-Condon factors for these calculations were computed using FCDYN, provided by A. Peluso.
[22] See, e.g., E. L. Sibert, W. P. Reinhardt, and J. T. Hynes, J. Chem. Phys. **81**, 1115 (1984); P. Brumer, in *Encyclopedia of Modern Physics*, edited by R. A. Meyers (Academic, New York, 1990), pp. 205–230.
[23] P. Christopher, M. Shapiro, and P. Brumer (unpublished).
[24] For example, V. Stert, P. Faramanara, and W. Randloff, J. Chem. Phys. **112**, 4460 (2000).